Absorption and Scattering 2D Volcano Images from Numerically Calculated Space-weighting functions

Edoardo Del Pezzo[1,2], Jesus Ibañez[2,3], Janire Prudencio[2,4], Francesca Bianco[1], Luca De Siena[5]

(1) Istituto Nazionale di Geofisica e Vulcanologia, sezione di Napoli Osservatorio Vesuviano. Via Diocleziano, 328. 80124 Napoli, Italy.
(2) Istituto Andaluz de Geofisica, University of Granada. Campus de Cartuja. Granada, Spain.
(3) Istituto Nazionale di Geofisica e Vulcanologia, Osservatorio Etneo. Piazza Roma, Catania, Italy.
(4) Department of Computer Science, Georgia State University, 25 Park Place SE, 30303 Atlanta, GA, USA
(5) University of Aberdeen, School of Geosciences, Dept. of Geology and Petroleum Geology. U.K..

Abstract

Short period small magnitude seismograms mainly comprise scattered waves in the form of coda waves (the tail part of the seismogram, starting after S-waves and ending when the noise prevails), spanning more than 70% of the whole seismogram duration. Corresponding coda envelopes provide important information about the earth inhomogeneity, which can be stochastically modeled in terms of distribution of scatterers in a random medium. In suitable experimental conditions (i.e. high earth heterogeneity) either the two parameters describing heterogeneity (scattering coefficient), intrinsic energy dissipation (coefficient of intrinsic attenuation) or a combination of them (extinction length and seismic albedo) can be used to image Earth structures. Once a set of such parameter couples has been measured in

a given area and for a number of sources and receivers, imaging their space distribution with standard methods is straightforward. However, as for finite-frequency and full-waveform tomography, the essential problem for a correct imaging is the determination of the weighting function describing the spatial sensitivity of observable data to scattering and absorption anomalies. Due to the nature of coda waves, the measured parameter-couple can be seen as a weighted space average of the real parameters characterizing the rock volumes illuminated by the scattered waves. This paper uses the Monte Carlo numerical solution of the Energy Transport Equation to find approximate but realistic 2D space-weighting functions for coda waves. Separate images for scattering and absorption based on these sensitivity functions are then compared with those obtained with commonly-used sensitivity functions in an application to data from an active seismic experiment carried out at Deception Island (Antarctica). Results show the that these novel functions are based on a reliable and physically grounded method to image magnitude and shape of scattering and absorption anomalies. Their extension to 3D holds promise to improve our ability to model volcanic structures using coda waves.

1 Introduction

It is well known since the pioneering works of Aki (1969), Latham et al. (1970), Aki and Chouet (1975), Sato (1977), Tsujiura (1978) that coda waves are generated by elastic scattering from earth heterogeneity. Short period seismic energy envelopes can thus be modeled in terms of scattering and intrinsic absorption parameters in statistically defined random Earth media. The solution of the Radiative Transfer integro-differential equation for scalar elastic waves (see e.g. Sato et al., 2012; Sato and Fehler, 2008) provides a suitable framework to describe these envelopes, including multiple scattering, as a function of source-receiver distance and time elapsed from the origin time of the event. Such a solution can be explicitly written in terms of scattering- and intrinsic absorption-coefficients, both of which characterize Earth's medium in areas crossed by coda waves, for a half space (Paasschens, 1997).

Recovering the effective spatial sampling of coda waves allows to locate and measure the magnitude of scattering and absorption anomalies in 2D and 3D media, therefore increasing our ability to unveil heterogeneous Earth

structures and interpret them in geological terms (Sato et al., 2012), contributing to complete the interpretation of total-attenuation images based on the measure of total-Q of direct P- and S- waves (see e.g. Prudencio et al. 2015b).

Estimates of intrinsic and scattering coefficients carried out at several source-receiver pairs using dense networks of seismic sensors generally show large spatial fluctuations and strong dependence of the two parameters on the source-receiver path. For waves crossing the Japanese crust and upper mantle, Carcolé and Sato (2010) observe striking examples of these effects. Measuring the real sensitivity of coda waves to spatial changes of attenuation coefficients is therefore a suitable way to image strong lateral fluctuations and to correlate them with tectonic structures, yielding geological hints on the area under study.

However, coda wave imaging has been grounded till now on very simple assumptions. Xie and Mitchell (1990) describe a back-projection method based on the single scattering model. These authors assume that the parameter deduced by using coda envelopes (Coda Q, see eq. 8 in Appendix) is representative of the attenuation averaged inside a scattering ellipse (see section 'Scattering Ellipse' in Appendix for definitions). Similar assumptions have been utilized by Calvet et al. (2013) who studied the area of Pyrenees and by De Siena et al. (2014) at Mt. St. Helens volcano. These authors assume that Coda Q is only sensitive to the structures crossed by the source receiver paths and spatially smooth their final 2D images by interpolating Coda Q values at the eight nearest nodes.

Several studies have proposed more complete and physically grounded approaches which go beyond first-order scattering approximations associated with average sensitivity inside the scattering ellipsoid. Pacheco and Snieder (2005) show how a single weak velocity anomaly perturbing a diffusive medium produces a measurable change in the coda travel time, deriving a 2D sensitivity function able to locate such an anomaly.De Siena et al. (2013) model envelopes of seismic traces in volcanic areas using 2D Radiative Transfer theory equations and diffusive boundary conditions in the presence of tomographically-measured high-scattering materials. Mayor et al. (2014) calculate 2-D sensitivity kernels for coda waves in the assumption of isotropic scattering and Margerin et al. (2016) in case of anisotropically scattering media. The two above papers describe a rigorous theoretical approach evaluating the relative intensity variations of coda caused by a localized scattering/absorption anomaly in the framework of Radiative Transfer Theory.

Their results are mainly focused at mapping the spatial changes in attenuation on the base of coda wave observations from distributed sources recorded at a seismic network and can be used to both locate single anomalies and to discriminate absorption from scattering properties.

Recently, Prudencio et al. (2013a) have used a back-projection method based on an empirical space weighting function of the attenuation parameters at given lapse times. Despite the observed improvement in resolution, the Gaussian weighting function assumed by Prudencio et al. (2013a) is only a reasonable approximation of the true sensitivity. In the present study a method for obtaining a weighting function (in 2D but extendable in 3D) based on the Montecarlo solution of the Radiative Transfer Theory is described. The sensitivity of the method to earth structures as well as the imaging potential of the approach is compared with those of different imaging methods by their concurrent application to active seismic data recorded at Deception Island volcano in Antarctica.

[1]

2 Method

Seismic energy envelopes are well described by the Radiative transfer model (Sato et al., 2012; see equation (4) for 2D and (5) for 3D, Section 'Scattering models, Seismic Albedo and Extinction Length' in Appendix) which is well approximated by the diffusion equation for highly inhomogeneous earth media. This study proposes a Monte Carlo approach to solve this equation and obtain space weighting functions suitable to estimate and image different attenuation parameters from coda waves. Following the scheme of Yoshimoto (2000), the total seismic energy is simulated assuming that a number, N, of energy particles is emitted randomly but isotropically from the source. When a single particle encounters a scatterer, it changes direction randomly in the interval 0 - 2π (isotropic scattering). The probability that a particle of unit energy at the source, E_0, encounters a scatterer is given by $\eta_s vt$, where $\eta_s = B_0 L e^{-1}$; at each interaction the fraction of its energy, $E/E_0 = 1 - Exp[\eta_i vt]$, where $\eta_i = Le^{-1}(1 - B_0)$, is absorbed by the propagation medium and transformed into heat (for symbol definitions

[1] Throughout this paper the syntactic rules used in Wolfram-Mathematica software for the use of parentheses are used: square brackets indicate the argument of a function; curly brackets indicate the elements of a matrix; round brackets indicate an algebraic grouping.

see Section 'Glossary of symbols' and equations (6) in Appendix). After a random number of collisions, the particle reaches the receiver at a given lapse time measured from the origin time, t. The energy envelope is finally obtained by the time histogram of all the particles arriving at the receiver. The value of the energy envelope (at a given lapse time) is thus the sum of the energies carried out by the particles at the end of all the scattering process, altogether arriving in a small time interval around t. The details of this procedure are reported in Yoshimoto (2000).

Numerous tests (e.g. Del Pezzo and Bianco, 2010, and references therein) demonstrate that the synthetic energy envelopes calculated with this method assuming an homogeneous ($v = constant$) half space well reproduces the theory given by equation (5), Section 'Scattering models, Seismic Albedo and Extinction Length' in Appendix.

The energy particles sample a portion of the propagation medium associated with the attenuation parameters used in the simulation. We thus heuristically consider the parameter couple of values calculated by the fit of energy envelope data to equation (5), as obtained via a back-projection in the area (volume in 3D) of earth medium sampled by the scattered waves through a weighted average operation (see the scheme of Figure 1). In different words, the elements of area crossed by more particles weight more in the back-projection procedure.

The weighting functions are determined in the following steps. The synthetic envelope obtained in the simulation is described by two parameters, one proportional to the density of the scatterers, $\eta_s = \frac{2\pi f}{vQ_s}$, and the other, $\eta_i = \frac{2\pi f}{vQ_i}$, representing intrinsic absorption (see also the definitions above in this Section). Given a couple of values $\{\eta_s, \eta_i\}$, the coordinates of the particle position and the scattering event positions (the points where collisions occur) at any time-step in the simulation are stored in two separate memory registers. At the end of the simulation procedure, the spatial density of collisions, $n_{sc}[x, y]$, and the path spatial density, $n_i[x, y]$, are calculated: n_{sc} and n_i are respectively the number of *collisions* and paths in an area $\Delta x \Delta y$, where Δx and Δy are small coordinate increments; These two quantities are both proportional to the probability that $\Delta x \Delta y$ affects the scattering and intrinsic attenuation tuning the energy envelope. n_i and n_{sc} are thus used as weighting functions in the back-projection method.

In Figure 2 the 2D space weighting functions calculated with this method are shown for the source-receiver configuration and parameters reported in

Table 1. It is noteworthy that in the range of ηs values used for our simulations, the value of η_i is inessential for the determination of the space weighting functions, as it modifies the absolute values without affecting the form of the weighting function. *tlapse* is set at 15 seconds as this is the maximum (max) lapse time used in data analysis. It is important to notice here that the max lapse time determines the dimension of the scattering ellipse and hence the resulting mapping. For different values of maximum lapse time, new simulations should be carried out in order to re-calculate the weighting functions.

Parameter	Value
η_i	$0.0km^{-1}$
η_s	$0.628km^{-1}$
δt	$0.05s$
t_{lapse}	$15s$
x_s	$0.0km$
y_s	$0.0km$
x_r	$5.0km$
y_r	$0.0km$
v	$2km/s$

Table 1. Parameters tuning the weighting functions shown in Figure 2. δt is the time step used in the simulation. t_{lapse} is the coda lapse time. $x_{s,}y_s$ and x_r, y_r are source and receiver coordinates respectively.

The two spatial distributions n_i and n_{sc} , calculated in 2D, are quite similar to each other for a wide set of $\{\eta_i, \eta_s\}$ physically-meaningfull couples. In principle, n_i and n_{sc} should be calculated for any couple of η_i and η_s values experimentally measured. However, calculating these two parameters for a number of $\{\eta_i\ \eta_s\}$ couples suitable to stabilize the tomography images is highly time-consuming. To speed up the procedure, an identical pattern for both n_{sc} and n_i is assumed: $n_{sc} = n_i = n$; then, a simple function of space coordinates and of $\{\eta_i\ ,\ \eta_s\}$ parameters, best fitting n for a large suite of $\{\eta_i, \eta_s\}$ couples, is calculated by trial-and-error. The explicit form of this approximating function has been evaluated in the following way.

The numerical weighting functions are first calculated using the Monte Carlo method for a wide set of feasible parameters and distances, setting the source at the origin and receiver at a point on the horizontal axis, at a distance D from the source. While it is observed that the shape of the weighting functions is insensitive to η_i, it is clear that it depends on η_s and D. This is

the reason why we set the value of η_i at a low arbitrary value ($\eta_i = 0.0001$) in all simulations. We calculated a suite of weighting functions considering D spanning from 5 km to 20 km and η_s spanning from 0.8 to 0.04, typical values measured in volcanoes (Sato et al., 2012). The calculation was carried out for a maximum lapse time of 15 seconds, using $3 \cdot 10^5$ energy particles and a half-space constant velocity, $v = 2.0$ km/s. Finally we found a function that fits well the 'average' shape of the weighting functions normalized at their value at the middle point between source and receiver via a trial and error approach. The function

$$
\begin{aligned}
f[x, y, x_r, y_r, x_s, y_s, \delta_x, \delta_y] = \frac{1}{4\pi\delta_x D^2 \delta_y} Exp\left[-\frac{\left(x - \frac{x_r + x_s}{2}\right)^2}{2\left(\delta_x D\right)^2} + \frac{\left(y - \frac{y_r + y_s}{2}\right)^2}{0.5\left(\delta_y D\right)^2} \right] + \\
\frac{1}{2\pi\delta_x D^2 \delta_y} Exp\left[-\frac{\left(x - x_s\right)^2}{2\left(\delta_x D\right)^2} + \frac{\left(y - y_s\right)^2}{2\left(\delta_y D\right)^2} \right] + \qquad (1) \\
\frac{1}{2\pi\delta_x D^2 \delta_y} Exp\left[-\frac{\left(x - x_r\right)^2}{2\left(\delta_x D\right)^2} + \frac{\left(y - y_r\right)^2}{2\left(\delta_y D\right)^2} \right]
\end{aligned}
$$

reasonably fits the numerical weighting functions with $\delta_x = \delta_y = 0.2$. δ_x and δ_y represent the spatial aperture of the weighting function. In Figure 2 the comparison between the numerical result and the analytical function (1) is shown as an example. The use of this approximation greatly reduces the computer time.

3 Separate Attenuation Images from Space Weighting Functions and test application to real data: Deception Island

Fitting equation (5 or 4, in Appendix) to the observed seismogram energy envelope for the single source-receiver path one can estimate the scattering and absorption coefficients in the equivalent couples of values $\{B_0\ ,\ Le^{-1}\}$ $\{Q_i^{-1}\ ,\ Q_S^{-1}\}$ or $\{\eta_i\ ,\ \eta_s\}$ all characterizing the medium in terms of intrinsic dissipation and scattering attenuation, respectively. The fitting procedure applied

to all the available source-receiver couples yields a data set suitable for imaging. Equation (5) can be substituted by mathematically simpler approximations like the single scattering approximation in case of a medium with mean free path much longer than the average source-receiver distance (equation 8; Section 'Scattering models, Seismic Albedo and Extinction Length' in Appendix), or the diffusion approximation in the opposite situation (see Sato et al., 2012 , equation 9; Section 'Scattering models, Seismic Albedo and Extinction Length' in Appendix). Details on the way of fitting the theoretical relationships (5,8or9) to the observed energy envelope data and the uncertainty associated with the parameter estimates can be found in Prudencio et al. (2013a).

The values of Q_i^{-1} and Q_s^{-1} for all the N source-receiver couples, ($\{1/Q_i^m, 1/Q_s^m\}$, where m ranges between 1 and N), represents the coda parameter set. In the $k-th$ space cell centered at the point of coordinates $\{x_k, y_k\}$ the probability that the true $Q_{i/s}^{-1}[x_k, y_k]$ represents the characteristic attenuation parameter of the cell $\{x_k, y_k\}$, is given by $1/Q_{i/s}^m \cdot n_m[x_k, y_k]$ where n_m is the $m-th$ weighting function, characteristic of the m-th source-receiver couple.

Its value is given thus by:

$$Q_{i/s}^{-1}[x_k, y_k] = \frac{\sum_m (1/Q_{i/s}^m) n_m[x_k, y_k]}{\sum_m n_m[x_k, y_k]} \tag{2}$$

Obviously, one can deduce maps of total attenuation, Q_T^{-1} , from those of Q_i^{-1} and Q_s^{-1}. As anticipated in the Introduction, an equivalent approach (based on Gaussian weighting functions) has been used to map the Q_i^{-1} and Q_s^{-1} space-distributions in Tenerife, Deception Island and Stromboli volcano (see Prudencio et al. , 2015a and references therein). In the following sections we test the approach and compare the results with those from methodologies currently used in literature.

An example of application of the present method to real data is provided using the active data set collected at Deception Island volcano in Antarctica already described by Prudencio et al. (2013b). We remark here that Prudencio et al. (2013b) used 15 seconds of max lapse time in the data analysis, the same value used in the present paper for the numerical simulations. This study provides an exhaustive description of data set and Gaussian weighting method used for 2D separate intrinsic- and scattering-attenuation imaging, which we review in the next Section. Results achieved using the present weighting functions in the 8 Hz frequency band are illustrated in Figure 3.

In Figure A1_a and A1_b (showing in the Appendix the spatial distributions of Q_i^{-1} and Q_s^{-1} respectively) we report the images obtained using the new weighting functions in different frequency bands.

4 Discussion

4.1 Comparison with Theoretical Sensitivity Kernels for coda wave interferometry and scattering tomography

The present method can be easily extended to 3D with an obvious inclusion of z in equation (2), and used in realistic earth models where velocity, v, and η_s are dependent on the spatial coordinates (Yoshimoto, 2000). The application of this method to a 3D space will be the topic of a forthcoming paper. The present weighting functions can be compared with the sensitivity kernels theoretically calculated for coda waves to locate the anomalies in the propagation medium detectable with coda wave interferometry. Mayor et al. (2014) suggest that their theoretically calculated sensitivity kernels for coda waves (see Section 'Sensitivity kernels calculated by Mayor et al. (2014)' in Appendix) could be used for both locating attenuation anomalies and for mapping separately lateral variations in the crust. In Figure 3 we reproduce the theoretical sensitivity kernels defined by Mayor et al. (2014) , K^{sc} and K^{int} (see Section 'Sensitivity kernels calculated by Mayor et al. (2014)' in Appendix for definitions), for the parameters in Table 1. K_{sc} has been demonstrated to be useful for greatly improving Nishigami's method (Nishigami, 1991), for searching for the spatial distribution of scatterers (Mayor et al., 2014); Margerin 2015, written communication), while K_{int} has been recently employed to map Q_i^{-1} measured in the Alps from Q_c^{-1} estimated for any source-receiver couple (Mayor et al., 2016). We wish to remark here that n_i and n_{sc} have been derived in a purely empirical way, based on considerations already reported in the section Method. The observation that the overall shape of n_{sc} calculated in the present paper is completely different from that of K_{sc} make us cautious about the ability of n_{sc} to describe the true scattering sensitivity. On the other hand, we have searched a weighting function for the spatial back-projection of Q_i^{-1} and Q_s^{-1}, jointly estimated from the single seismogram, in the assumption of diffusion regime. We found, using heuristical considerations based on numerical simulations of coda Energy en-

velopes, that in the diffusion regime the spatial density of collisions takes the same functional shape of the spatial density of elementary paths. We thus empirically decided to use this functional shape to image both intrinsic and scattering attenuation parameter distribution.

4.2 Comparison with results achieved using different weighting functions

The results obtained using the present weighting function n (n-images) have been compared with those obtained using the Gaussian weighting function (Prudencio et al. 2013b) (g-images), the strip-like weighting functions used by Calvet et al. (2013) and De Siena et al. (2014) (s-images) and the middle-point between source and receiver as described by Singh and Herrmann (1983) and by Jin and Aki (1988) (m-images). This comparison is shown in Figure 4. The mathematical form of the weighting function used for g-images is described in Prudencio et al. (2013a). It is a Gaussian-like space function, centered at the middle point between source and receiver, with a rapid lateral decay. s-images are obtained using as weighting function a 2-D boxcar, 1km large around the source-receiver path (Calvet et al., 2013). To obtain the m-images we space averaged the measured values attributed to the middle point of the source-receiver segment, in a square ($1km$ side) moving eastward and northward with steps of 0.5 km and eventually drawing the isolines. The different panels in Figures A2 show that the choice of the weighting functions modifies the results, introducing blurring effects. In particular, the m-images show less space smoothing than those calculated using the other methods. The apparently increased resolution is a numerical artifact in this last case.

4.3 Resolution tests

Both checkerboard and anomaly tests have been carried out to test the method proposed in the present paper. Being n_i and n_{sc} similar in the present assumptions we carry on the tests for a generic inverse quality factor, Q^{-1}. The input data for the tests were calculated on the base of the checkerboard (or anomaly) Q^{-1} input values (see color scale in Figure 5). The procedure we have used can be summarized in the following steps: 1) for any source receiver couple we calculate the space weighting function using equation (1) (n-images), the Gaussian weighting function (g-images) and the

strip-like weighting function (s-images). 2) we multiply the weighting functions thus calculated for the space distribution of test values (checkerboard or spike) and calculate their weighted average. We use a grid-step of 0.5 km for both checkerboard and spike test. 3) We use the weighted average as input data set for the tests. Squared cells in the checkerboard test have a side of 3km; the center cell in the anomaly test is 4 km wide. 4) After applying the present method to all the source-receiver couples, for any space coordinate couple we have thus a set of weighted Q^{-1} values. Their weighted average corresponds to the output value. We also calculate the arithmetical average inside the scattering ellipse (m-images).

Results are shown in Figures 5 and 6 where in the output the percent changes respect to the space average of the input values are plotted. While the present method does not well represent the absolute input values, it clearly depicts their space variations. It is notewhorthy that the feature of checkerboard input is preserved for the n-images even for a low contrast (a factor 2) among the Q values in the input cells (see panels e and f in Figure 5).

A comparison of the present n-images with the g-images and s-images is reported. Both (n) and (g) outputs show similar results, with a good determination of the checkerboard anomalies in the 3km x 3 km cell, while the (s) output shows instead decreasing resolution with some blurring. The bias introduced by an approximate weighting function is thus unimportant for g-images while significant for s-images. In this last case s-images underestimate the real imaging capability.

We remark that no resolution test can be calculated for the mid-point images (m), as the resolution for these images is completely determined by the space averaging process underlying the method. By using the present weighting functions the anomaly test nicely reproduces the input anomaly in all cases, while border effects (brown color in the northeastern sector) are reduced with respect to the result of the other methods.

5 Conclusions

In the present study, we propose the use of weighting functions n_i and n_{sc} for coda wave back-projection mapping computed via Monte Carlo solutions of the Energy Transport theory equations. Using single-station active recordings and a simpler gaussian equivalent of the proposed weighting functions,

recent studies were able to separate intrinsic from scattering attenuation at Deception Island (Prudencio et al. 2013b), Tenerife (Prudencio et al. 2013a) and Stromboli (Prudencio et al. 2015a) volcanoes.

The Gaussian shape of the function used in the above-mentioned works is centered at the middle point between source and receiver and presents a sharp (and somewhat arbitrary) lateral decay both for scattering-Q and for intrinsic-Q imaging. The resolution and reliability of the novel weighting functions are tested on the Deception dataset used by Prudencio et al. (2013b) and subsequently compared with those of a) the Gaussian-like weighting function, b) the strip-like weighting function Calvet et al. (2013), and c) the middle-point weighting function Jin and Aki (1988). The novel weighting function described in the present paper are based on an reliable physical model; on the other hand the Gauss-like function shows similar results in terms of shape and value of the anomalies. The difference in shape and, especially, the value of the anomalies becomes instead relevant when using the strip-like and middle-point functions. Being the results obtained at Tenerife, Deception Island and Stromboli based on the Gauss-like functions, it can be inferred that they are therefore affected by minor biases that do not change the final interpretation of the anomalies. Nevertheless, the approach presented here, even heuristical, is grounded on the solution of equations representing the physics that underlies different attenuation mechanisms and it should be therefore preferred to the others.

Appendix

Glossary of symbols

Symbol	Explanation
N	Number of wave-particles in the simulation
η_s	Scattering coefficient. $g = \eta_s = \frac{2\pi f}{vQ_s}$ where f is the frequency
v	Wave speed
t	Lapse time (measured from origin)
η_i	Intrinsic attenuation coefficients. $\eta_i = \frac{2\pi f}{vQ_i}$ where f is the frequency
B_0	Seismic Albedo. $B_0 = \frac{\eta_s}{\eta_i + \eta_s}$
Le	Extinction Length. $Le^{-1} = \eta_i + \eta_s$
n_{sc}, n_i	Space density of scatterers and paths, respectively
$\{x_s, y_s\}$	Source coordinates
$\{x_r, y_r\}$	Receiver coordinates
r	$\sqrt{(x_s - x_r)^2 + (y_s - y_r)^2}$ source-receiver distance
δt	time step used in simulations
Q_i, Q_s	Intrinsic and Scattering Quality Factor
K^{sc}, K^{iso}, K^{int}	Sensitivity Kernels for coda waves in Mayor et al. (2014)
E^{2D}, E^{3D}	2-D and 3-D Energy envelopes, numerically evaluated
E^{2D}_{SS}, E^{3D}_{SS}	Single-Scattering 2-D and 3-D Energy envelopes
P_i,P	Probability

Scattering Ellipse

The scattering ellipse in 2D for a source located at $\{-x_d, 0\}$ and a receiver at $\{x_d, 0\}$ is defined as:

$$\frac{x^2}{(\frac{vt_{lapse}}{2})^2} + \frac{y^2}{(\frac{vt_{lapse}}{2})^2 - \frac{2x_d^2}{4}} = 1 \tag{3}$$

where t_{lapse} is the maximum coda lapse time.

Scattering models, Seismic Albedo and Extinction Length

The seismogram energy envelopes are well described by the Radiative transfer model (Sato et al., 2012). The approximate solution of the Radiative Transfer

Equation (RTE) in 2 dimensions (Sato et al., 2012) is:

$$E^{2D}[r,t] = \frac{W_0 exp[-Le^{-1}vt]}{2\pi rv}\delta[t-\frac{r}{v}] + W_0 H[t-\frac{r}{v}]\cdot\frac{B_0 Le^{-1}}{2\pi vt}(1-\frac{r^2}{v^2t^2})^{-1/2}$$

$$exp[B_0 Le^{-1}\sqrt{v^2t^2-r^2}]exp[-Le^{-1}vt] \tag{4}$$

and in 3 dimensions Paasschens (1997):

$$E^{3D}_{ij}[r,t] \approx \frac{W_0 exp[-Le^{-1}vt]}{4\pi r^2 v}\delta[t-\frac{r_{ij}}{v}] + W_0 H[t-\frac{r_{ij}}{v}]\cdot\frac{(1-\frac{r_{ij}^2}{v^2t^2})^{1/8}}{(\frac{4\pi vt}{3B_0 Le^{-1}})^{3/2}}\cdot$$
$$exp[-Le^{-1}vt]F[vtB_0 Le^{-1}(1-\frac{r_{ij}^2}{v^2t^2})^{3/4}] \tag{5}$$

where $F[x] = e^x\sqrt{1+2.026/x}$; W_0 is the energy at source; v is the wave speed in the half-space; H is the Heaviside function; δ is the Dirac's delta. B_0 and Le^{-1} represent the Seismic Albedo and the Extinction Length inverse, respectively. They can be expressed in terms of quality factor, Q, by

$$B_0 = Q_T/Q_S \tag{6}$$

and

$$Le^{-1} = \frac{2\pi f}{v}\left(\frac{1}{Q_S}+\frac{1}{Q_i}\right) \tag{7}$$

Where $Q_T^{-1} = Q_i^{-1} + Q_S^{-1}$.

In 3-D the single (isotropic) scattering the approximate solution is (Zeng et al., 1991)

$$E^{3D}_{SS}[r,t] = W_0\frac{ln\left[\frac{1+r/vt}{1-r/vt}\right]}{4\pi rvt}B_0 Le^{-1}H[t-r/v]exp\left[-Le^{-1}\right] \tag{8}$$

Using this model it is almost impossible to obtain separate estimates of B_0 and Le^{-1} due to the respective trade-off; consequently, researchers generally measure the quantity $Le^{-1} = \frac{2\pi f}{v}(Q_i^{-1}+Q_s^{-1})$. $Q_i^{-1}+Q_s^{-1}$, the sum of the

Q-inverses, is called Q_c or Coda Q. It is noteworthy that Q_c represents total-Q only when single-scattering approximation is valid. In the opposite case (diffusion approximation) the approximate solution is (Zeng, 1991)

$$E_D^{3D}[r,t] = H[t-r/v]\left(\frac{3B_0Le^{-1}}{4\pi vt}\right)^{3/2} exp\left[-\frac{3}{2}\frac{r^2B_0Le^{-1}}{vt} - vt(Le^{-1}-B_0Le^{-1})\right] \tag{9}$$

Sensitivity kernels calculated by Mayor et al. (2014).

The effects of the spatial distribution of scatterers giving rise to anomalies in coda envelope have been investigated by Pacheco and Snieder (2005) and more recently by Mayor et al. (2014). In this section their approach is briefly reviewed.

The first basic consideration is that the borders of the sensitivity zone are given by the scattering ellipse (see 3) which delineates the maximum area (in 2D) encompassed by the scattered waves. Pacheco and Snieder (2005) calculated the space probability of the scattered energy recorded in the seismogram between the coda start-time and the maximum lapse time considered, T. These authors introduce the concept of probability for a single wave-particle, contributing to form the wave energy envelope at the receiver, to pass at lapse time, t', in $\mathbf{x}$. For a source located at $\mathbf{s}$ and a receiver at $\mathbf{r}$, and recording the particle at its arrival at time t , this probability is

$$P_i[\mathbf{x}[t'],\mathbf{r},\mathbf{s},t] = P_i[\mathbf{x}[t'],\mathbf{s}]P_i[\mathbf{r},\mathbf{x}[t'],t-t'] \tag{10}$$

where i represents the i-th particle, and the right hand side of is the product of the probability that a particle arrives at position $\mathbf{x}$ at time t', and that scatters and finally arrives at the receiver $\mathbf{r}$ at lapse time t. The sum, $P[\mathbf{x}[\mathbf{t}'],\mathbf{r},\mathbf{s},t]$, over the set of N particles represents the whole wave packet; P defines the probability that a wave packet from s arrives at distance r and at time t. Integrating this quantity over the space V

$$P[r,s,t] = \int_V P[\mathbf{x},\mathbf{r},\mathbf{s},t]dV[\mathbf{x}] \tag{11}$$

where the variable t' drops out as it depends on $\mathbf{x}$. Finally, the probability that the diffuse (scattered) energy arrives at the receiver located at position

$\mathbf{r}$ in a time interval from origin time to T, and due to a scatterer in the position $\mathbf{x}$ is:

$$K[\mathbf{x},\mathbf{r},\mathbf{s},T] = \frac{1}{P[\mathbf{r},\mathbf{s},T]}\int_0^T P[\mathbf{r},\mathbf{x}[\mathbf{t}'],t-t']P[\mathbf{s},\mathbf{x}[\mathbf{t}'],t']dt' \qquad (12)$$

Equation (12) from Pacheco and Snieder (2005) can be used to locate the elastic perturbation affecting the intensity of the diffusive field in which coda wave observations are carried out. Pacheco and Snieder (2005) equal P to the formulation of the radiation intensity in 2D given by the solution of Radiative Transfer Equation (equation 4).

Mayor et al. (2014) suggest the possibility to locate single anomalies and to discriminate between their absorption or scattering characteristics. The sensitivity kernels for a constant velocity 2-D earth medium and isotropic multiple scattering are:

$$K^{sc}[\mathbf{x},\mathbf{r},\mathbf{s},T] = K^{iso}[\mathbf{x},\mathbf{r},\mathbf{s},T] + K^{int}[\mathbf{x},\mathbf{r},\mathbf{s},T] \qquad (13)$$

where K^{sc} is the scattering sensitivity kernel, K^{int} is the intrinsic-dissipation sensitivity kernel which will be defined hereafter, and K^{iso} is given by

$$K^{iso}[\mathbf{x},\mathbf{r},\mathbf{s},T] = \int_0^T P[\mathbf{r},\mathbf{x}[\mathbf{t}'],t-t']P[\mathbf{s},\mathbf{x}[\mathbf{t}'],t']dt' \qquad (14)$$

All the other symbols were already defined above. It is noteworthy that equation 14 is analogous to equation 12 except for the normalization constant. Finally, K^{int} is given by

$$K^{int}[\mathbf{x},\mathbf{r},\mathbf{s},T] = -\frac{1}{2\pi}\int_0^{2\pi}\int_0^{\frac{vTB_0}{Le}} K1[\mathbf{x},\mathbf{r},\mathbf{s},T]K2[\mathbf{x},\mathbf{r},\mathbf{s},T]dt'd\alpha \qquad (15)$$

with $K1$ and $K2$ given by

$$K1[\mathbf{x},\mathbf{r},\mathbf{s},T] = exp[-(tt-tt')\delta[\mathbf{R}' + (tt-tt')\hat{\mathbf{n}}']\Phi[\mathrm{tt}-\mathrm{tt}'] + \qquad (16)$$

$$+ \frac{exp[\sqrt{(tt-tt'-R')} - (tt-tt')]\Phi[tt-tt'-R']}{2\pi(tt-tt'+\mathbf{R}'.\hat{\mathbf{n}'})} \qquad (17)$$

and

$$K2[\mathbf{x},\mathbf{r},\mathbf{s},T] = exp[-tt'\delta[\mathbf{R_0}-tt'\hat{\mathbf{n}}']\Phi[\mathrm{tt}'] + \frac{\exp[\sqrt{\mathrm{tt}'^2-\mathrm{R}_0^2}]\Phi[\mathrm{tt}'-\mathrm{R}_0]}{2\pi(\mathrm{tt}'-\mathbf{R}_0.\hat{\mathbf{n}'})} \tag{18}$$

where δ is the Dirac's delta distribution, $tt = B_0 Le^{-1} vt$; $tt' = B_0 Le^{-1} vt'$; $\mathbf{R}' = \{\mathbf{x}-\mathbf{r}\}$; $\mathbf{R_0} = \{\mathbf{x}-\mathbf{s}\}$; $\hat{\boldsymbol{n}'} = \{Cos[\alpha], Sin[\alpha]\}$; R' and R are the magnitudes of vectors $\mathbf{R}'$ and $\mathbf{R}$. In the above equations the intrinsic quality factor of equation (7) is set at infinity, to simplify the discussion. This affects only the overall amplitude of the functions but not their space pattern (Mayor et al., 2014). K^{int} is negative, as it represents the energy that is subtracted from the wave field and transformed into heat.

All the details relative to equations (16) and (18) are explained in Mayor et al. (2014). The theoretical kernels can be calculated only in the assumptions of constant velocity.

Figure Captions

1. Figure 1. An energy particle starts its random path (dashed lines) at the source (star), encounters several scatterers (grey circles), and arrives at the receiver (star). At the maximum lapse time, t_{lapse}, the scatterers are located at the border of the scattering ellipse (black line).

2. Figure 2. n_i and n_{sc} functions numerically calculated with the parameters in Table 1. Upper two panels: isolines of n_i and n_{sc} normalized at their value in the middle of source - receiver distance. Medium and lower panels represent the section in the planes x=0.0, x=2.5 x=5.0 and y=0.0. Blue lines represent n_{sc}; orange lines represent n_i. The red line represents the approximation calculated with equation (1) while the dashed black line represents the Gauss-weighting function used by Prudencio et al. (2013b) and the dashed green line the Strip-like function used by Calvet et al. (2013).

3. Figure 3. K^{sc} and K^{int} (see Appendix for definitions and details) kernel sections, plotted as a function of distance on vertical normal planes disposed along source-receiver direction (y=0) and through the middle distance point ($x = 0.0$), the source location position ($x = -2.5$),

and the receiver position ($x = 2.5$). To the quantity K^{int} we superimpose the correspondent quantity n_{sc} (or n_i) approximated by equation (1) [red line], the Gauss-weighting function used by Prudencio et al. (2013b) [black dashed] and the Strip-like function used by Calvet et al. (2013) [dashed green line] for an easy comparison.

4. Figure 4. Results calculated applying the weighting functions discussed in the present paper to the measures of Q_i^{-1} and Q_s^{-1} at Deception Island (n-image). g-image, s-image and m-image are the images obtained using the gauss-like weighting, the strip-like weighting and the middle point weighting functions, respectively. The coast line of Deception Island (ticker black curve) is superimposed on each plot.

5. Figure 5. Checkerboard test for n-images (the present method), g-images (Gaussian weighting) and s-images (strip function weighting). Panels b, c, d represent the test for the checkerboard input shown in panel a (a contrast in Q of a factor 20). Panel f report the n-image output for the input shown in panel e (a contrast in Q of a factor 2)

6. Figure 6. Spike test for a n-, g- and s-images.

7. Figure A1_nqi. Frequency-dependent 2D Deception Island model calculated applying the weighting functions discussed in the present study to the single-station measurements of Q_i^{-1} (n-image).

8. Figure A1_nqs. Frequency-dependent 2D Deception Island model calculated applying the weighting functions discussed in the present study to the single-station measurements of Q_s^{-1} (n-image).

9. Figure A2_gqi. Frequency-dependent 2D Deception Island model calculated applying the gaussian-like weighting functions to the single-station measurements of Q_i^{-1} (g-image).

10. FigureA2_gqs. Frequency-dependent 2D Deception Island model calculated applying the gaussian-like weighting functions to the single-station measurements of Q_s^{-1} (g-image).

11. FigureA2_sqi. Frequency-dependent 2D Deception Island model calculated applying the strip-like weighting functions to the single-station measurements of Q_i^{-1} (s-image).

12. FigureA2_sqs. Frequency-dependent 2D Deception Island model calculated applying the strip-like weighting functions to the single-station measurements of Q_s^{-1} (s-image).

13. FigureA2_mqi. Frequency-dependent 2D Deception Island model calculated applying the middle-point weighting functions to the single-station measurements of Q_i^{-1} (m-image).

14. FigureA2_mqs. Frequency-dependent 2D Deception Island model calculated applying the middle-point weighting functions to the single-station measurements of Q_s^{-1} (m-image).

Acknowledgements

Yosuke Aoki and an anonimous reviewer greatly improved the quality of the paper. All calculations were made with Mathematica-10^{TM}. Discussions with Marie Calvet, Danilo Galluzzo, Mario La Rocca, Salvatore De Lorenzo, Jessie Mayor, Ludovic Margerin are gratefully acknowledged. The authors are supported by MEDSUV European project and by Spanish Project Project Ephestos, CGL2011-29499-C02-01. The TIDES EU travel Cost action provided travel money to support cooperation between Luca De Siena and the other authors.

References

Aki, K. (1969). Analysis of the Seismic Coda of Local Earthquakes as Scattered Waves. *Journal Of Geophysical Research-Solid Earth 74*(2), 615–631.

Aki, K. and B. Chouet (1975). Origin of coda waves: Source, attenuation, and scattering effects. *Journal Of Geophysical Research-Solid Earth 80*(23), 3322–3342.

Calvet, M., M. Sylvander, L. Margerin, and A. Villasenor (2013). Spatial variations of seismic attenuation and heterogeneity in the pyrenees: Coda q and peak delay time analysis. *Tectonophysics 608*, 428–439.

Carcolé, E. and H. Sato (2010). Spatial distribution of scattering loss and intrinsic absorption of short-period S waves in the lithosphere of Japan

on the basis of the Multiple Lapse Time Window Analysis of Hi-net data. *Geophysical Journal International 180*(1), 268–290.

De Siena, L., E. Del Pezzo, C. Thomas, A. Curtis, and L. Margerin (2013, October). Seismic energy envelopes in volcanic media: in need of boundary conditions. *Geophysical Journal International 195*(2), 1102–1119.

De Siena, L., C. Thomas, G. P. Waite, S. C. Moran, and S. Klemme (2014, November). Attenuation and scattering tomography of the deep plumbing system of Mount St. Helens. *Journal Of Geophysical Research-Solid Earth 119*(11), 8223–8238.

Del Pezzo, E. and F. Bianco (2010). Two-layer earth model corrections to the MLTWA estimates of intrinsic- and scattering-attenuation obtained in a uniform half-space. *Geophysical Journal International 182*(2), 949–955.

Jin, A. and K. Aki (1988). Spatial and temporal correlation between coda q and seismicity in china. *Bull Seismol Soc Am 78*(2), 741–769.

Latham, G., M. Ewing, F. Press, G. Sutton, J. Dorman, Y. Nakamura, N. Toksoz, R. Wiggins, J. Derr, and F. Duennebier (1970, January). Passive seismic experiment. *Science 167*, 455 – 457.

Margerin, L., T. Planes, J. Mayor, and M. Calvet (2016). Sensitivity kernels for coda-wave interferometry and scattering tomography: theory and numerical evaluation in two-dimensional anisotropically scattering media. *Geophys. J. Int. 204*, 650–666.

Mayor, J., M. Calvet, L. Margerin, O. Vanderhaeghe, and P. Traversa (2016). Crustal structure of the alps as seen by attenuation tomography. *Earth and Planetary Science Letters 439*, 71 – 80.

Mayor, J., L. Margerin, and M. Calvet (2014, April). Sensitivity of coda waves to spatial variations of absorption and scattering: radiative transfer theory and 2-D examples. *Geophysical Journal International 197*(2), 1117–1137.

Nishigami, K. (1991). A new inversion method of coda waveforms to determine spatial distribution of coda scatterers in the crust and uppermost mantle. *Geophysical Research Letters 18*(12), 2225–2228.

Paasschens, J. (1997). Solution of the time-dependent Boltzmann equation. *Physical Review E 56*, 1135–1141.

Pacheco, C. and R. Snieder (2005). Time-lapse travel time change of multiply scattered acoustic waves. *J. Acoust. Soc. Am. 118*(3), 1300 – 1310.

Prudencio, J., L. De Siena, J. M. Ibanez, E. Del Pezzo, A. Garcia Yeguas, and A. Díaz-Moreno (2015-b). The 3D Attenuation Structure of Deception Island (Antarctica). *Surveys in Geophysics 36*(3), 371–390.

Prudencio, J., E. Del Pezzo, A. Garcia Yeguas, and J. M. Ibanez (2013-a, November). Spatial distribution of intrinsic and scattering seismic attenuation in active volcanic islands - I: model and the case of Tenerife Island. *Geophysical Journal International 195*(3), 1942–1956.

Prudencio, J., E. Del Pezzo, J. Ibanez, E. Giampiccolo, and D. Patane (2015-a). Two-dimensional seismic attenuation images of stromboli island using active data. *Geophysical Research Letters 42*(doi:10.1002/2015GL063293.).

Prudencio, J., J. M. Ibanez, A. Garcia Yeguas, E. Del Pezzo, and A. M. Posadas (2013-b, October). Spatial distribution of intrinsic and scattering seismic attenuation in active volcanic islands - II: Deception Island images. *Geophysical Journal International*.

Sato, H. (1977). Single isotropic scattering model including wave convesions. *J.Phys.Earth*, 14.

Sato, H. and M. Fehler (2008, November). Earth Heterogeneity and Scattering Effects on Seismic Waves. *Advances in geophysics, Renata Dmowska Editor*, 1–445.

Sato, H., M. Fehler, and T. Maeda (2012). *Seismic wave propagation and scattering in the heterogeneous Earth Second Edition*. Springer.

Singh, S. and R. B. Herrmann (1983). Regionalization of crustal coda q in the continental united states. *Journal of Geophysical Research 88*(B1), 527–538.

Tsujiura, M. (1978). Spectral Analysis of the Coda Waves from Local Earthquakes. *Bulletin of the Earthquake Research Institute (Tokio)*.

Xie, J. and B. Mitchell (1990). A Back-Projection Method for Imaging Large-Scale Lateral Variations of Lg Coda Q with Application to Continental Africa. *Geophysical Journal International 100*(2), 161–181.

Yoshimoto, K. (2000). Monte Carlo simulation of seismogram envelopes in scattering media. *Journal Of Geophysical Research-Solid Earth 105*, 6153–6161.

Zeng, Y. (1991). Compact solutions for multiple scattered wave energy in time domain. *Bulletin Of The Seismological Society Of America*.

Zeng, Y., F. Su, and K. Aki (1991). Scattering wave energy propagation in a random isotropic scattering medium. Part 1. Theory. *Journal Of Geophysical Research-Solid Earth 96*, 607–619.

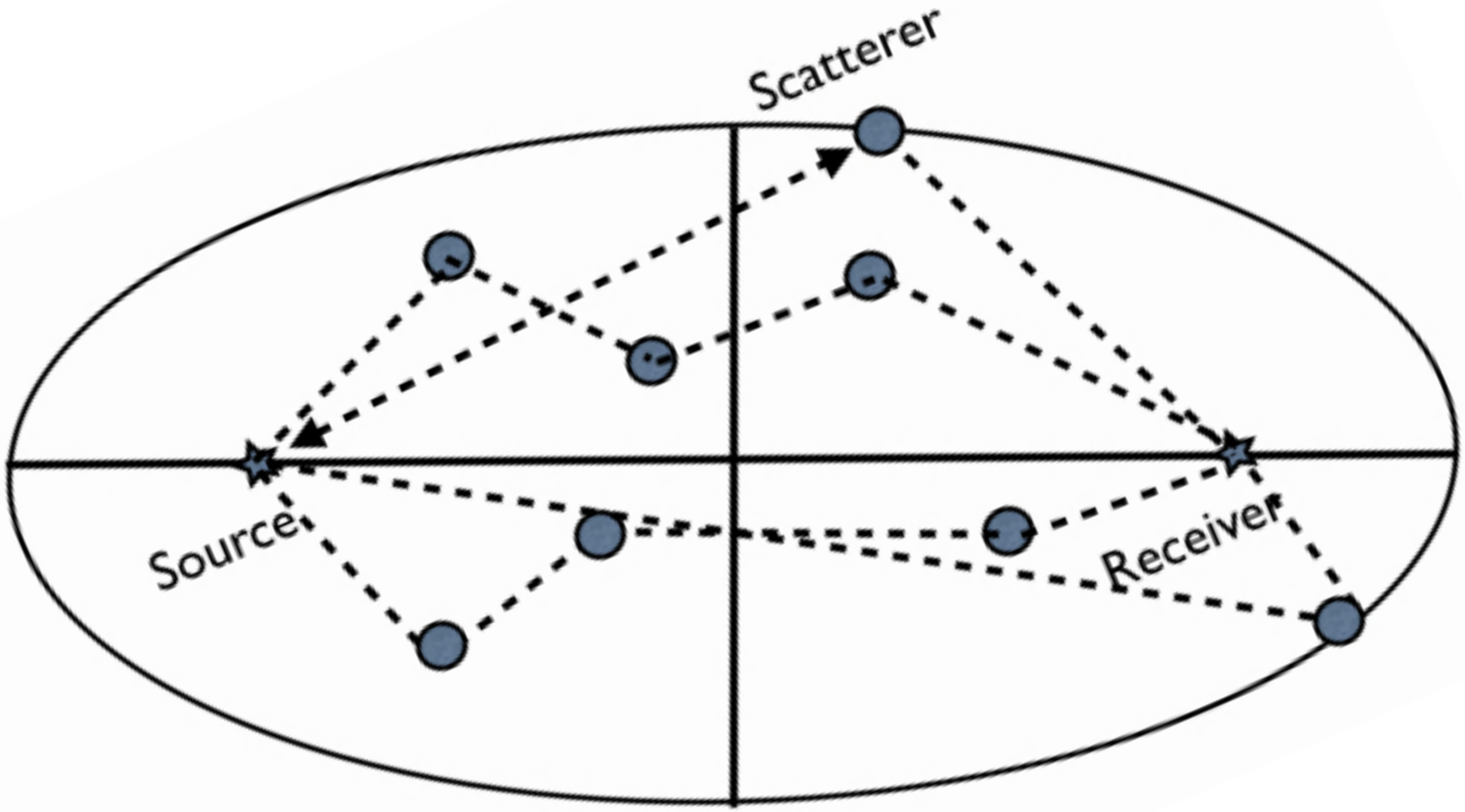

Figure 1 - An energy particle starts its random path (dashed lines) at the source (star), encounters several scatterers (grey circles), and arrives at the receiver (star). At the maximum lapse time, $t_{lapse,}$ the scatterers are located at the border of the scattering ellipse (black line).

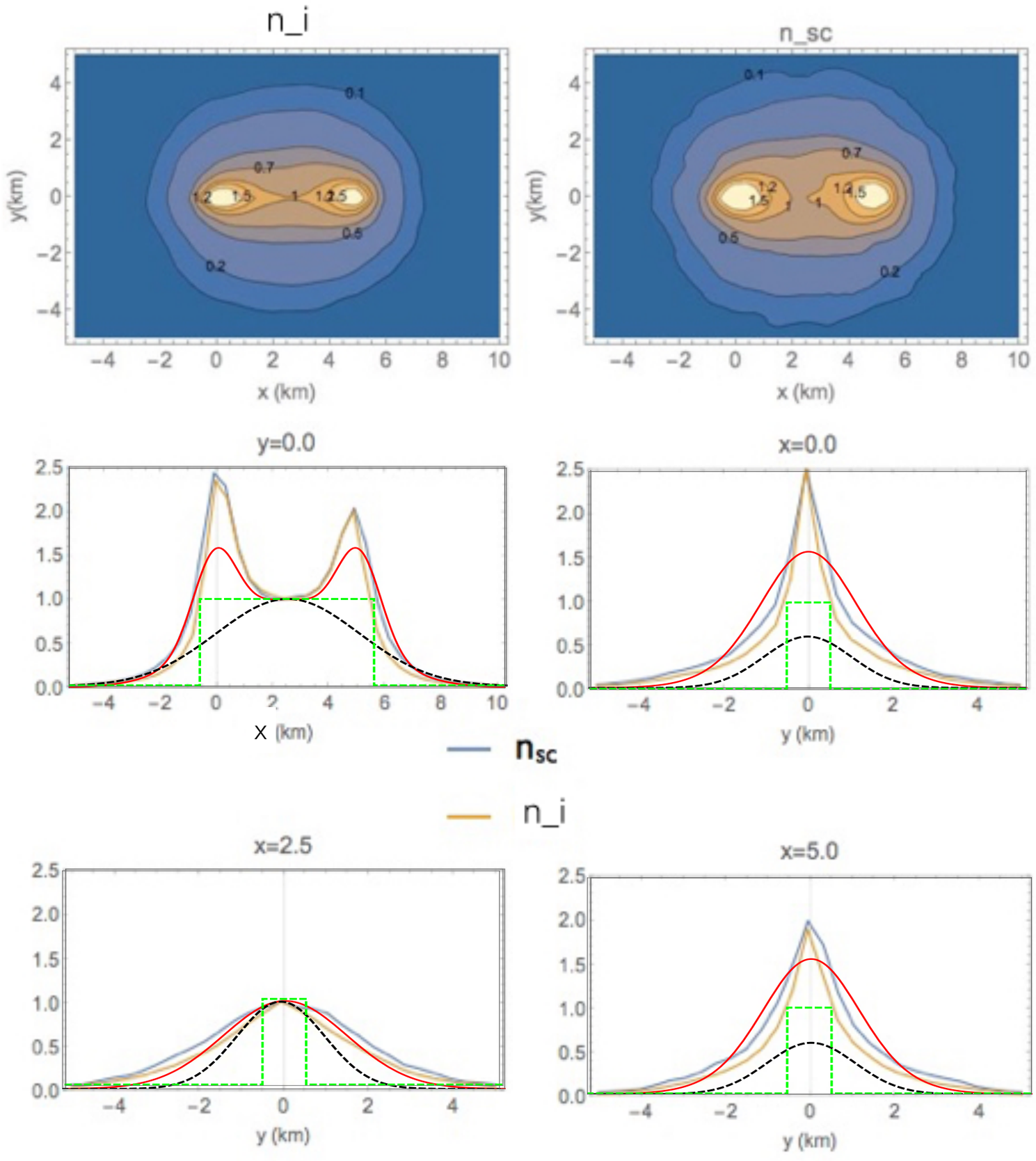

Figure 2. n_i and n_{sc} functions numerically calculated with the parameters in Table 1. Upper two panels: isolines of n_i and n_{sc} normalized at their value in the middle of source - receiver distance. Medium and lower panels represent the section in the planes x=0.0, x=2.5 x=5.0 and y=0.0. Blue lines represent n_{sc}; orange lines represent n_i. The red line represents the approximation calculated with equation (1) while the dashed black line represents the Gauss-weighting function used by Prudencio et al. (2013b) and the dashed green line the Strip-like function used by Calvet et al. (2013).

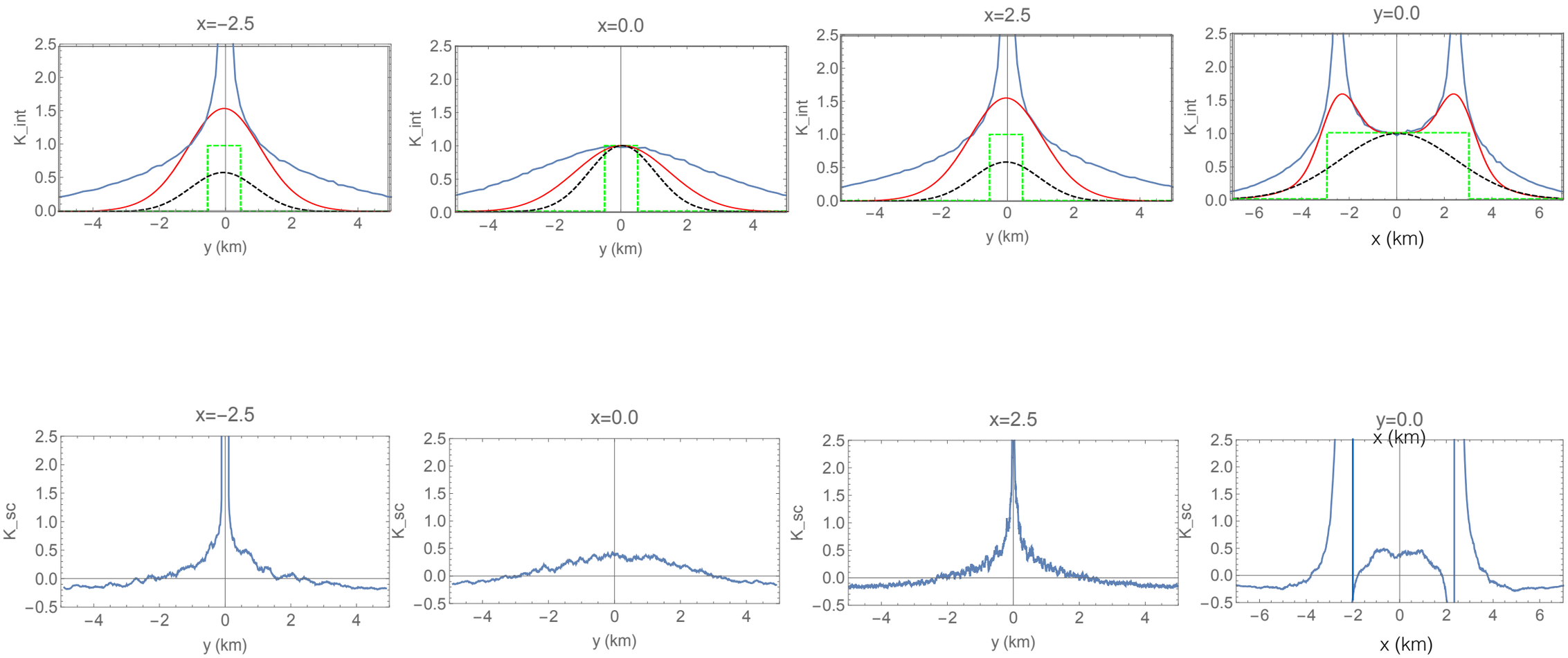

Figure 3. K_{sc} and K_{int} (see Appendix for definitions and details) kernel sections, plotted as a function of distance on vertical normal planes disposed along source-receiver direction (y=0) and through the middle distance point (x=0.0), the source location position (x=-2.5), and the receiver position (x=2.5). To the quantity K_{int} we superimpose the correspondent quantity n_i (or n_{sc}) approximated by equation (1) [red line], the Gauss-weighting function used by Prudencio et al. (2013 - b) [black dashed line] and the Strip-like function used by Calvet et al. (2013) [dashed green line] for an easy comparison.

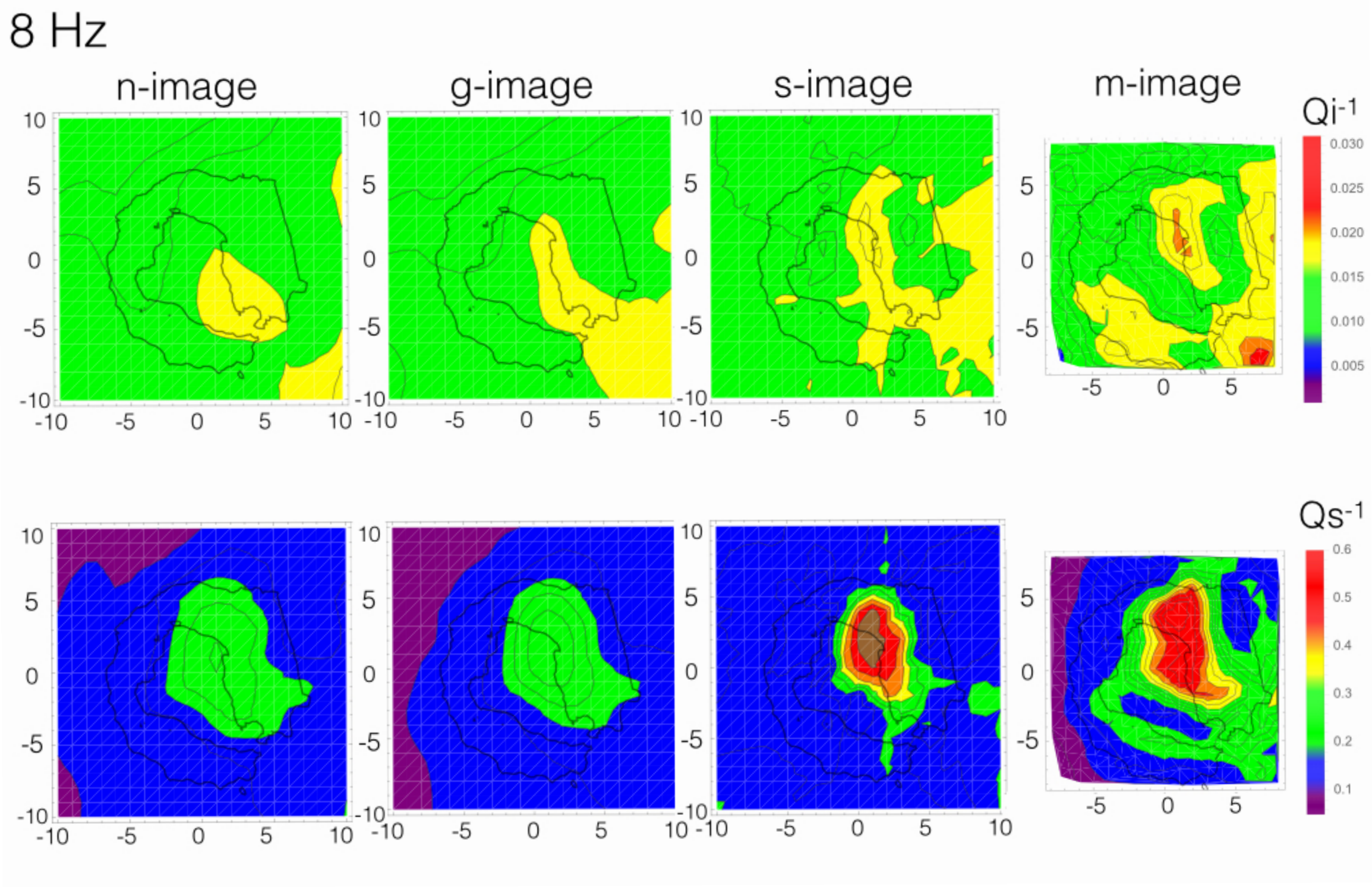

Figure 4 - Results calculated applying the weighting functions discussed in the present paper to the measures of Q_i^{-1} and Q_s^{-1} at Deception Island (n-image). g-image, s-image and m-image are the images obtained using the gauss-like weighting, the strip-like weighting and the middle point weighting functions, respectively. The coast line of Deception Island (ticker black curve) is superimposed on each plot.

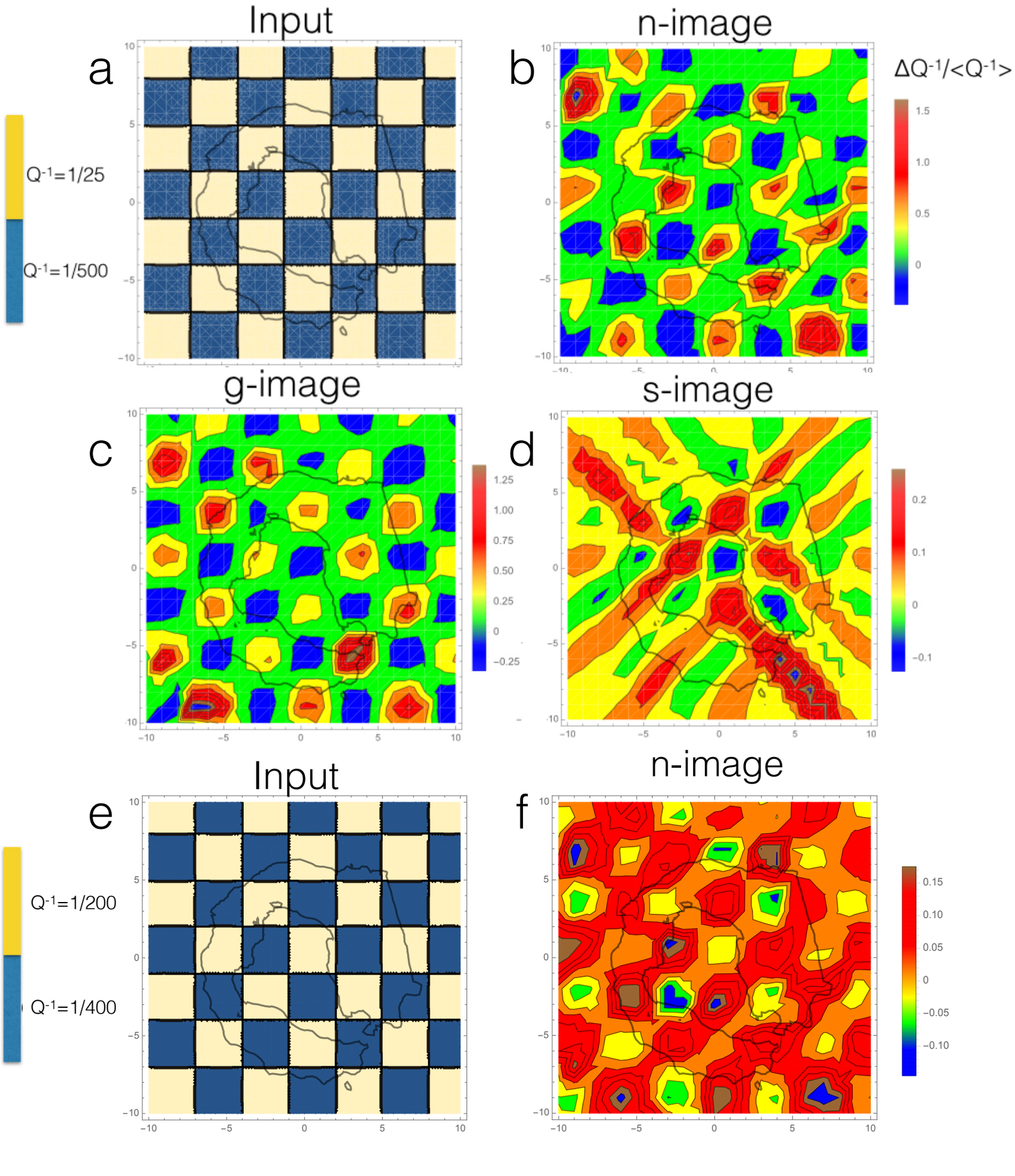

Figure 5 - Checkerboard test for n-images (the present method), g-images (Gaussian weighting) and s-images (strip function weighting). Panels b,c,d represent the test for the checkerboard input shown in panel a (a contrast of a factor 20). Panel f report the n-image output for the input shown in panel e (a contrast of a factor 2)

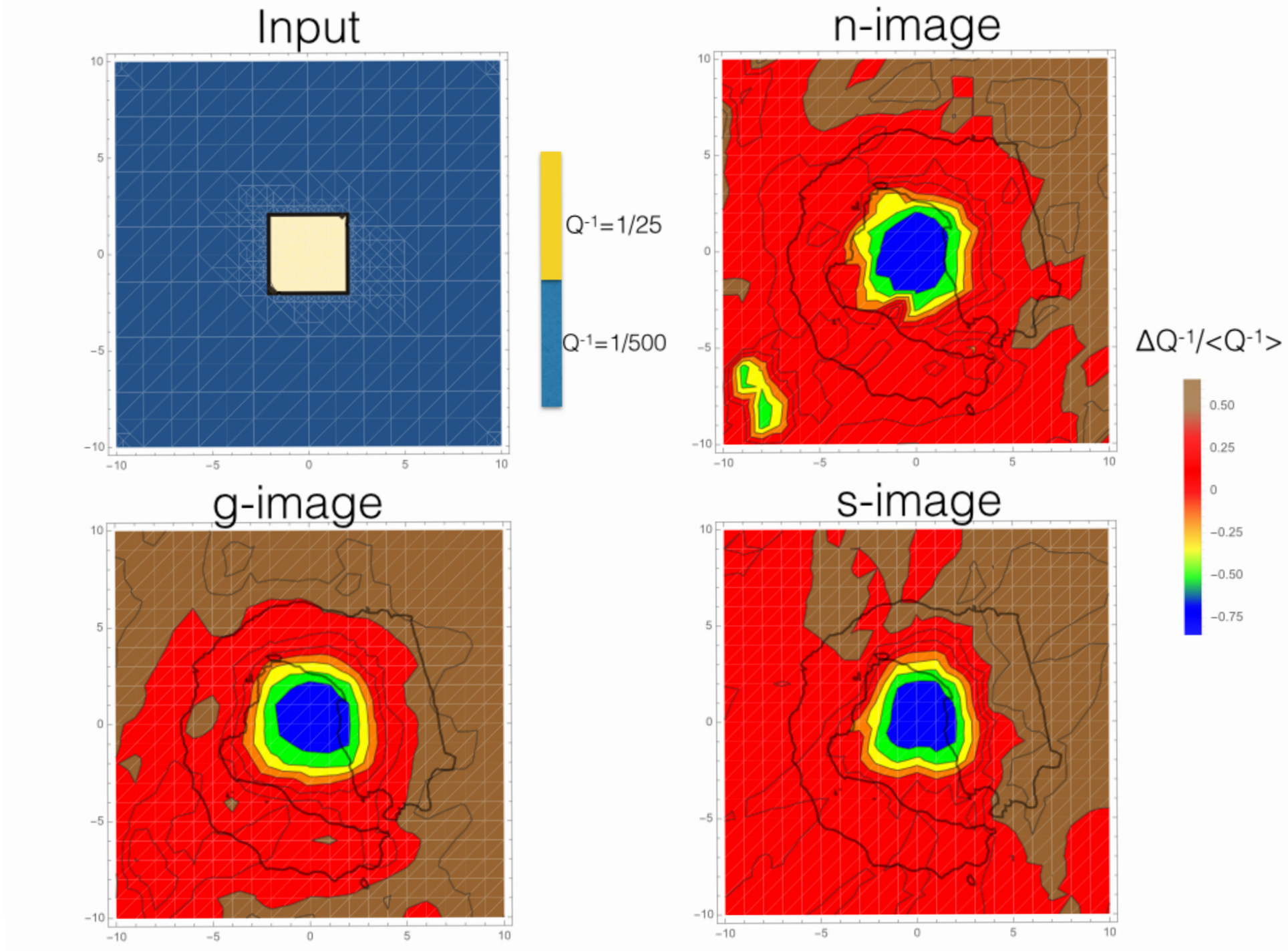

Figure 6 - Spike test for a n-, g- and s-images.

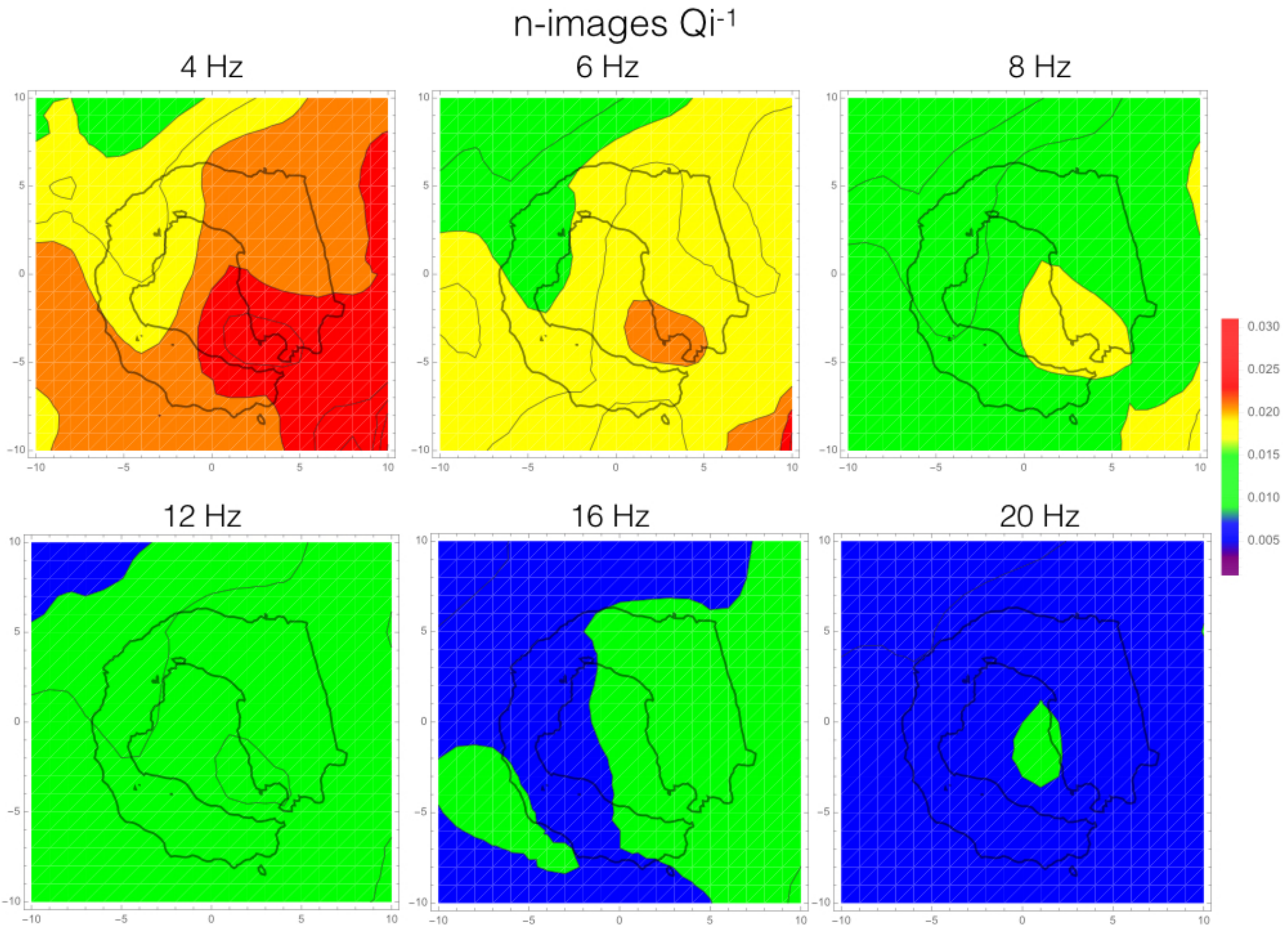

Figure A1_nqi - Frequency-dependent 2D Deception Island model calculated applying the weighting functions discussed in the present study to the single-station measurements of (n-image).

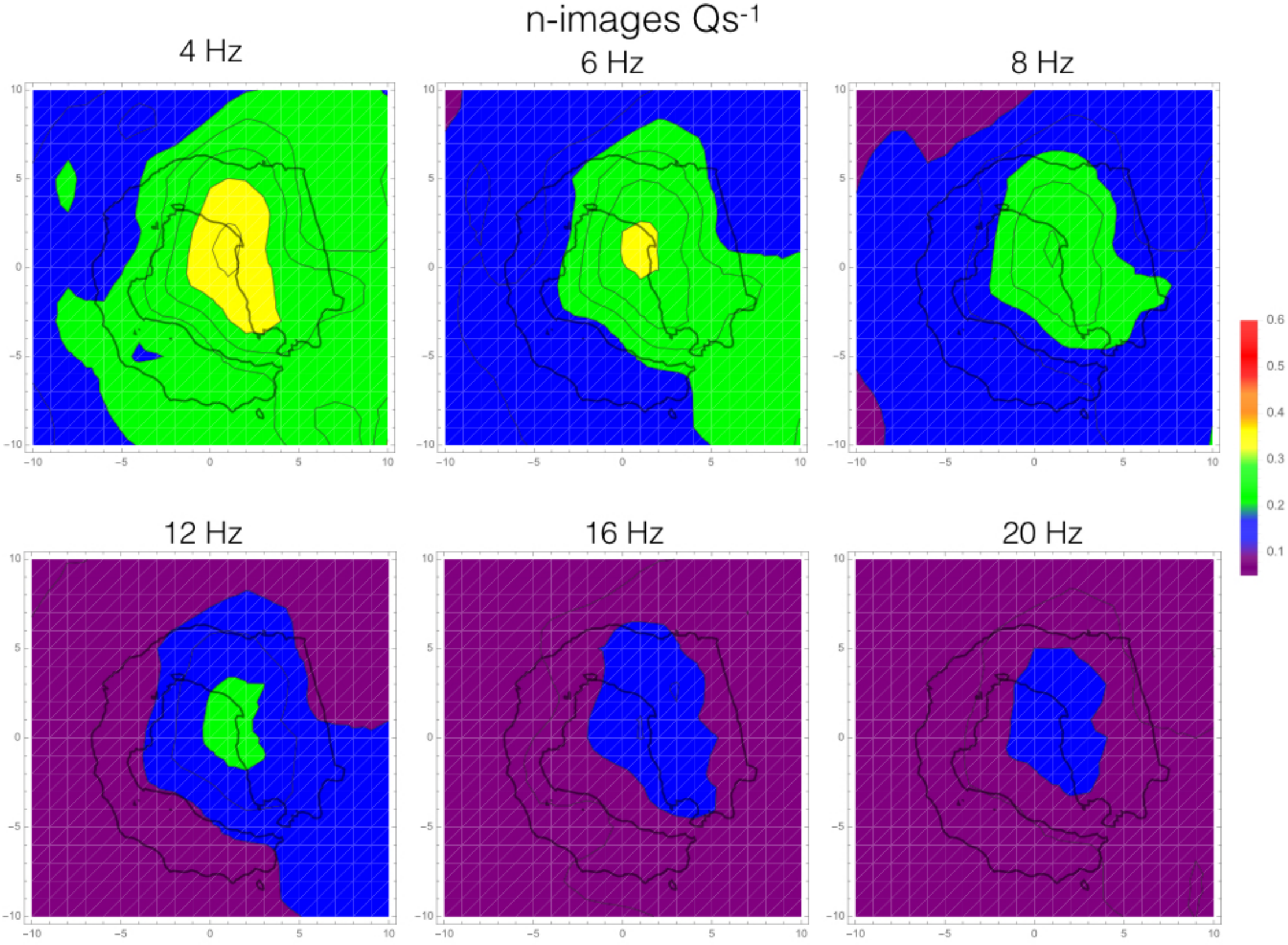

Figure A1_nqs - Frequency-dependent 2D Deception Island model calculated applying the weighting functions discussed in the present study to the single-station measurements Q_s^{-1} of (n-image).

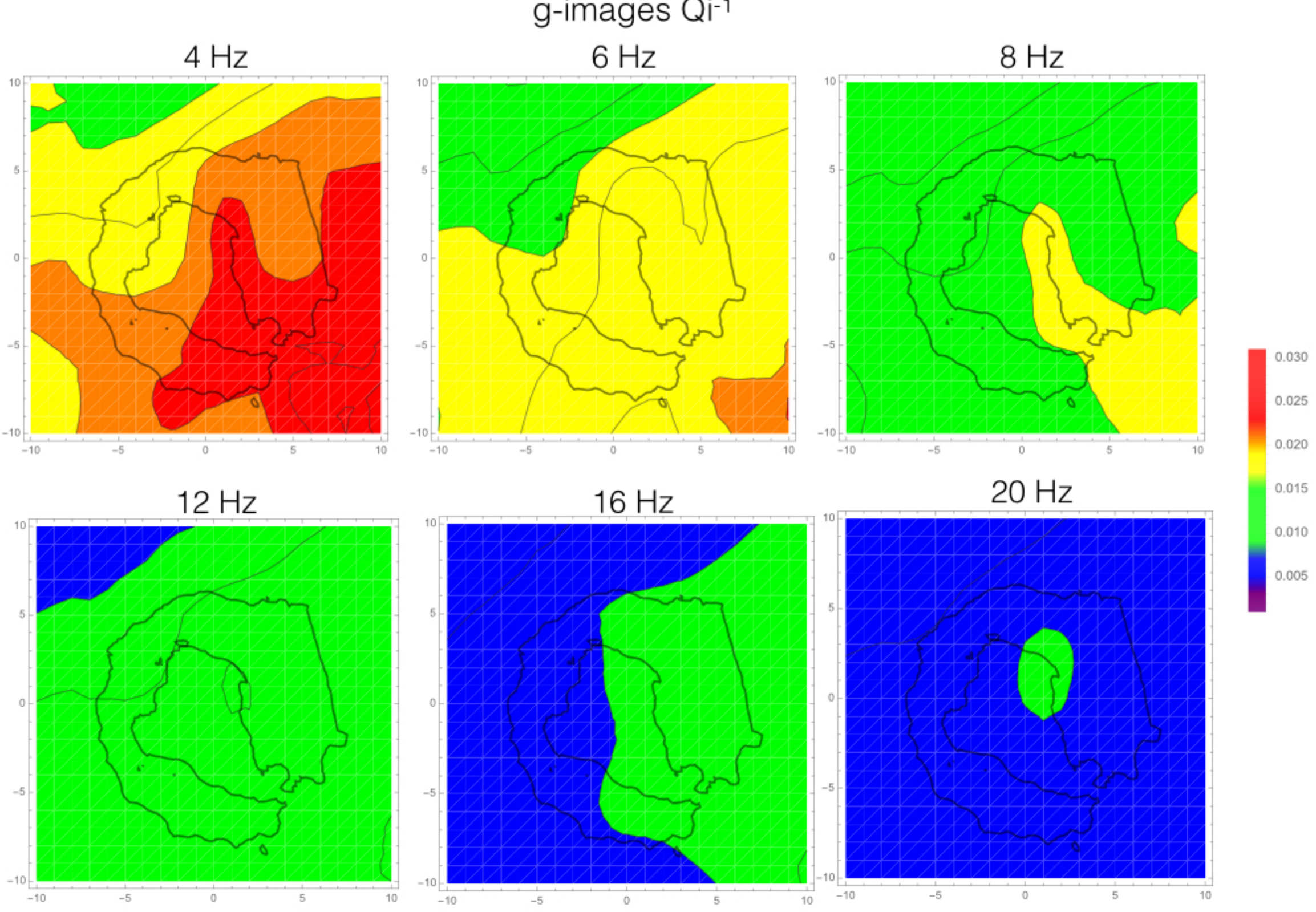

Figure A2_gqi - Frequency-dependent 2D Deception Island model calculated applying the gaussian-like weighting functions to the single-station measurements of Q_i^{-1} (g-image).

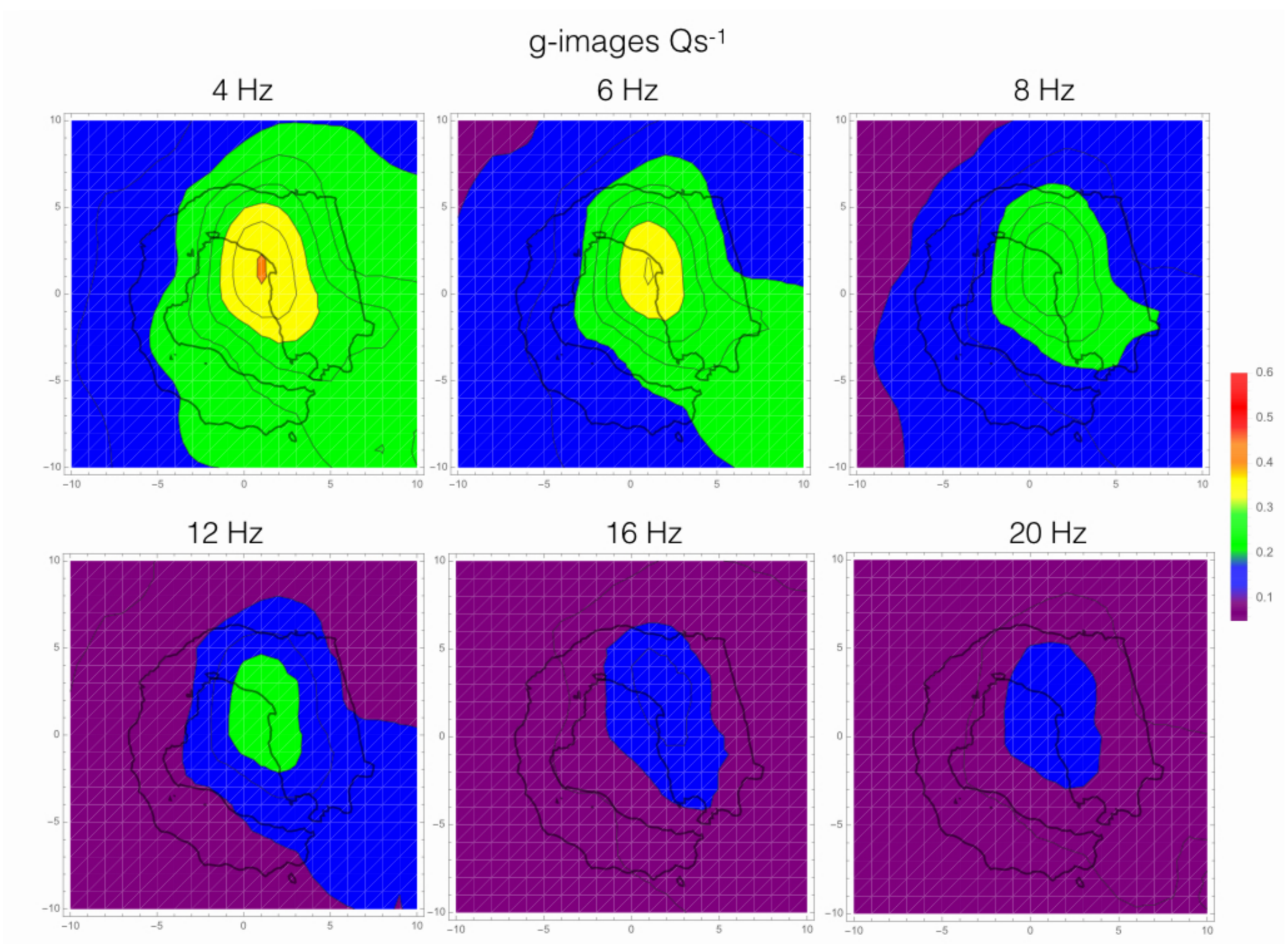

Figure A2_gqs - Frequency-dependent 2D Deception Island model calculated applying the gaussian-like weighting functions to the single-station measurements of Q_S^{-1} (g-image).

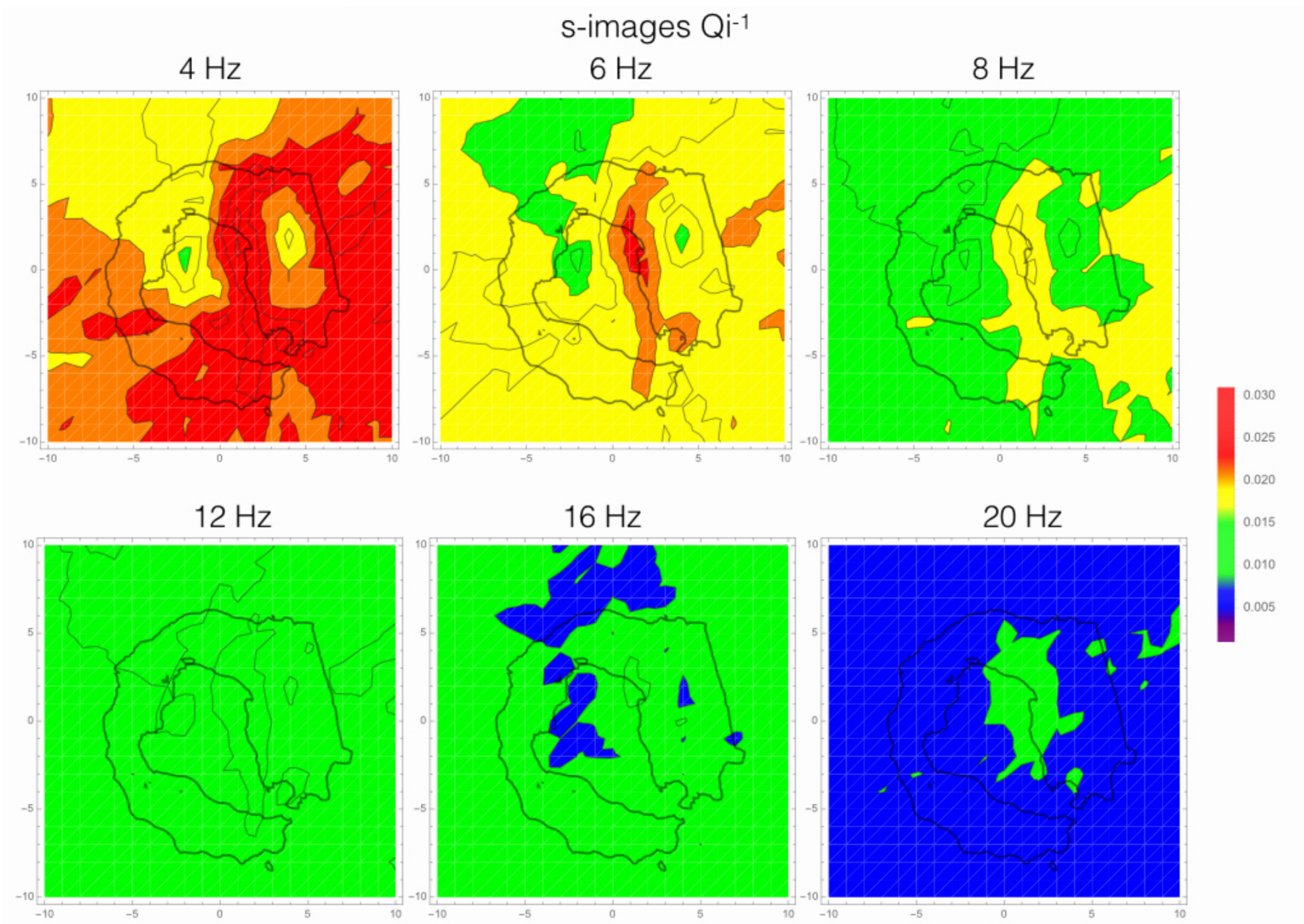

Figure A2_sqi - Frequency-dependent 2D Deception Island model calculated applying the strip-like weighting functions to the single-station measurements of Q_i^{-1} (s-image).

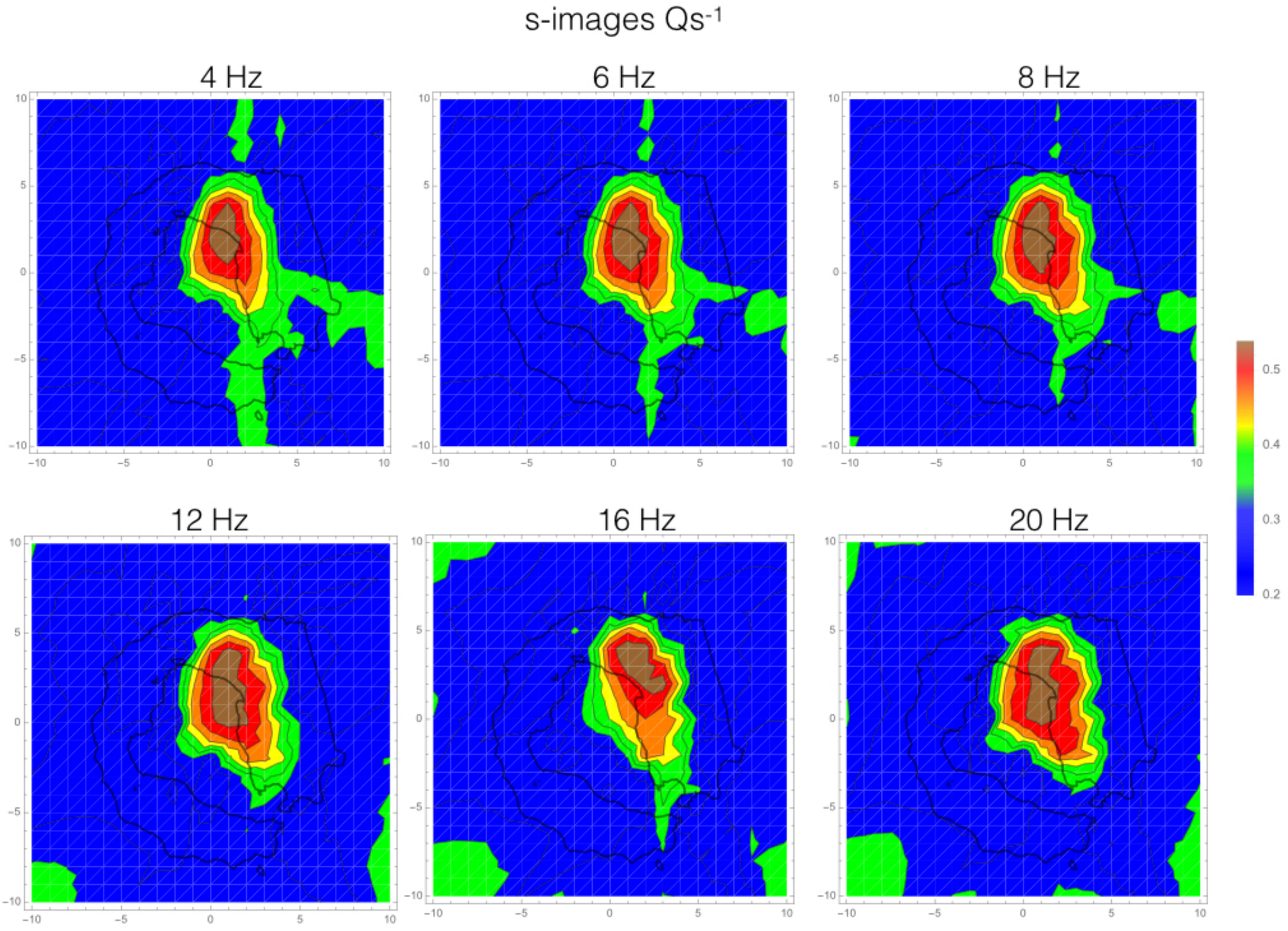

Figure A2_sqs - Frequency-dependent 2D Deception Island model calculated applying the strip-like weighting functions to the single-station measurements of Q_s^{-1} (s-image).

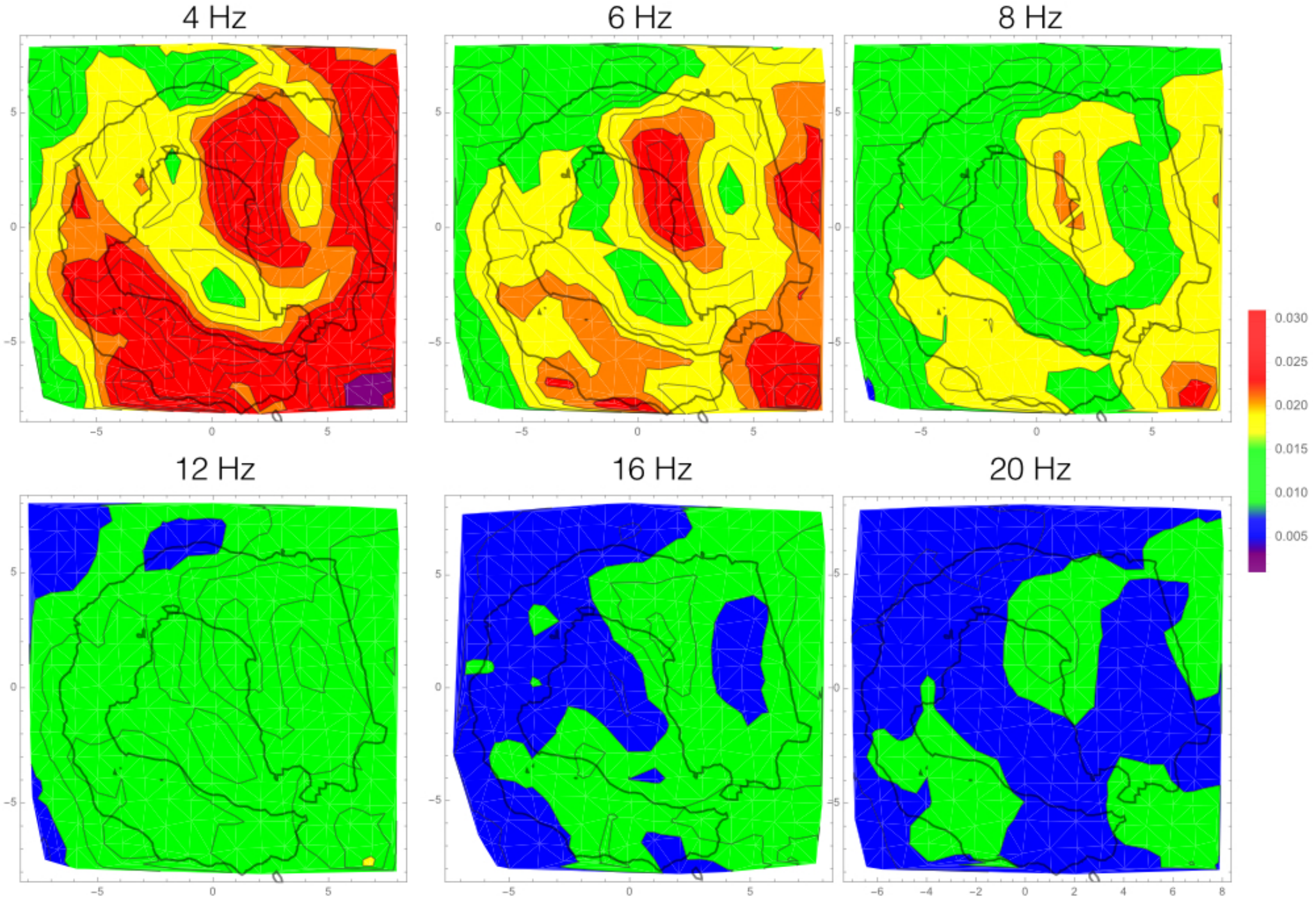

Figure A2_mqi - Frequency-dependent 2D Deception Island model calculated applying the middle-point weighting functions to the single-station measurements of Q_i^{-1} (m-image).

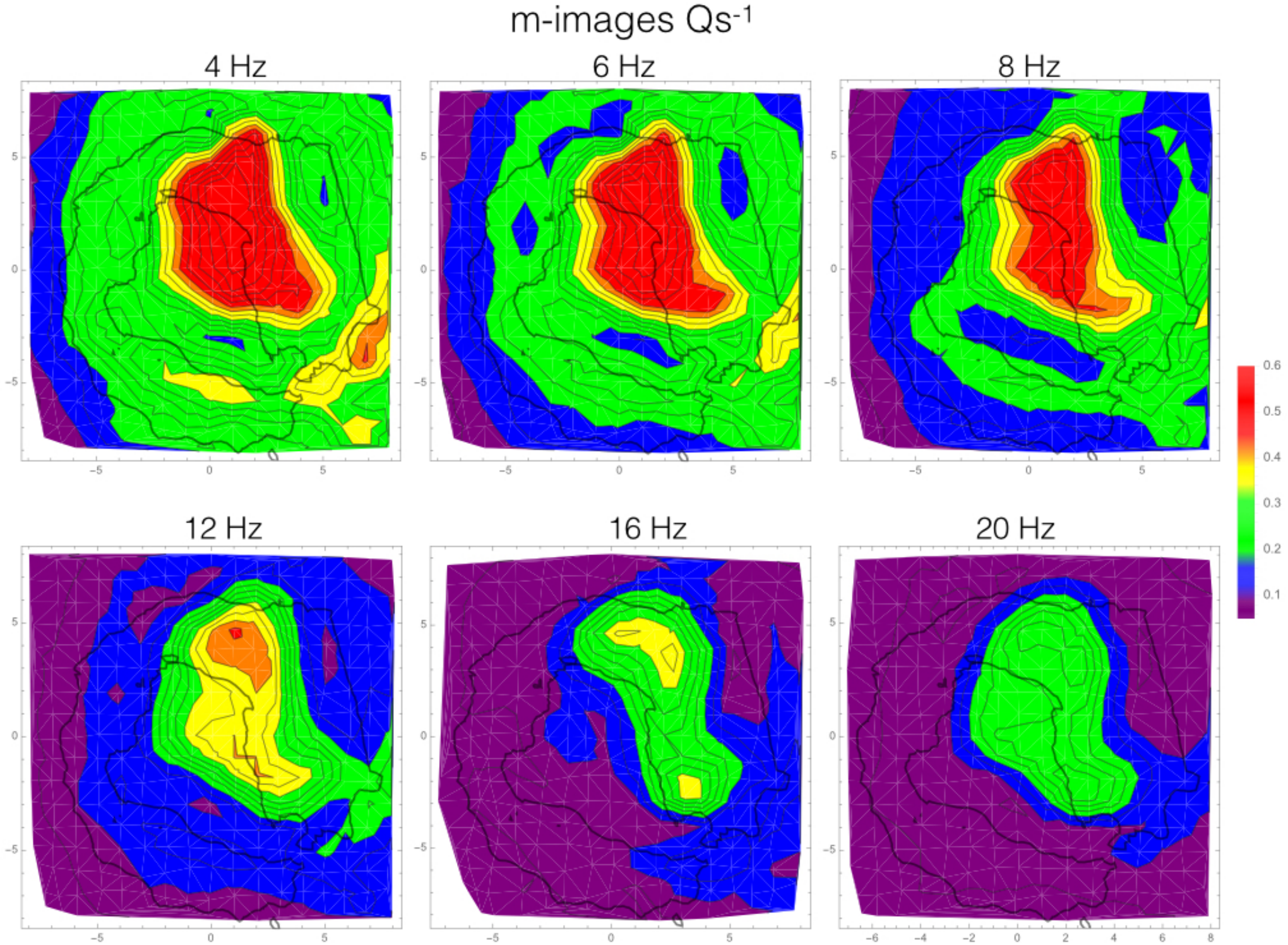

Figure A2_mqs - Frequency-dependent 2D Deception Island model calculated applying the middle-point weighting functions to the single-station measurements of Q_s^{-1}(m-image).